



Bioinspired composites from freeze casting with clathrate hydrates



Steven E. Naleway^{a,*}, Christopher F. Yu^b, Michael M. Porter^{a,1}, Arijit Sengupta^d, Peter M. Iovine^d, Marc A. Meyers^{a,b,c}, Joanna McKittrick^{a,b}

^a Materials Science and Engineering Program, University of California, San Diego, 9500 Gilman Drive, La Jolla, CA 92093, USA

^b Department of Mechanical and Aerospace Engineering, University of California, San Diego, 9500 Gilman Drive, La Jolla, CA 92093, USA

^c Department of NanoEngineering, University of California, San Diego, 9500 Gilman Drive, La Jolla, CA 92093, USA

^d Department of Chemistry and Biochemistry, University of San Diego, San Diego, CA 92110, USA

ARTICLE INFO

Article history:

Received 18 October 2014

Accepted 25 January 2015

Available online 7 February 2015

Keywords:

Clathrate hydrate

Bioinspired

Freeze casting

Ceramic matrix composite

Mechanical behavior

ABSTRACT

Freeze casting with isopropanol (IPA)–H₂O as a freezing agent has shown the potential to create porous scaffolds with enlarged pores. Though not experimentally proven, this effect has been suggested to be the result of non-stoichiometric structures called clathrate hydrates forming during the freezing process. In this manuscript, we build upon these results to provide experimental evidence of the formation of clathrate hydrates during the freeze casting process when using IPA–H₂O as a freezing agent and explain the observed maximum in pore area through observations of the enthalpy of the transitions. Additionally, these enlarged pores are harnessed in order to create two-phase bioinspired composites. These composites exhibit an increase in mechanical strength over both constituents, a phenomena that is common to complex biological composites. Previous reports have shown that the characteristic method of failure for many freeze cast scaffolds is buckling of the lamellar walls within the porous microstructure. It is proposed that this increase in mechanical strength is due to the support of the second phase, which resists this characteristic buckling failure mode.

© 2015 Elsevier Ltd. All rights reserved.

1. Introduction

Amongst the most common structural elements found within nature are layered two phase composites made up of interpenetrating ductile and brittle phases. These structures, for example, are found in mammalian bone [1], gastropod shells [2] and fish scales [3]. These composites are known for their excellent mechanical properties, which often exceed what would be expected from a simple mixture of their constituents [4]. As a result, there has been much research into bioinspired, two phase composite materials [5–7]. In most cases, to more closely mimic the nature of biological materials, these composites have consisted of ceramic and polymeric phases [5–7]. The freeze casting fabrication technique has been explored as a method to create such two phase composite materials [6,8,9].

The freeze casting process has been studied over the last decade due to its versatility, ease of use and inexpensive setup and operation [5,10,11]. Freeze casting is carried out by directional solidification, in a controlled manner, of a slurry made up of solid loading

(e.g. ceramic particulates) and a liquid freezing agent. The frozen scaffolds are then lyophilized (freeze dried) followed by sintering in order to form a final ceramic scaffold where the ice crystals have been converted into aligned pores and the solid loading has formed lamellar walls (when H₂O is utilized as the freezing agent) [5,10,11]. Altering the slurry properties through the solid loading [12,13] and liquid freezing agent [14,15] characteristics have been reported to alter the final scaffold microstructure. Additionally, control of the final scaffolds have been reported through the application of external forces and processes such as changing the freezing rate [16] and applying electric [17] and magnetic fields [18].

After fabrication, porous freeze cast scaffolds can be infiltrated with polymers or metal melts in order to form interpenetrating ceramic–polymer composites [6,19–21]. There are a number of reported polymer infiltration methods including: particle centrifugation [22], *in situ* polymerization [4,23] and polymer solvent evaporation [24]. Amongst these, the most commonly applied method is *in situ* polymerization where a liquid monomer and catalyst are infiltrated into a scaffold under vacuum and then allowed to polymerize [4,5,23].

The recent work of Porter et al. [14] demonstrated the effect of isopropanol (IPA) as an additive to freeze casting with TiO₂ as the solid loading. The resultant scaffolds showed a large increase in

* Corresponding author. Tel.: +1 541 255 9998; fax: +1 858 534 5698.

E-mail address: snaleway@eng.ucsd.edu (S.E. Naleway).

¹ Present address: Department of Mechanical Engineering, Clemson University, Clemson, SC 29634, USA.

pore area up to an observed maximum at 5 vol.% IPA. This increase in pore area was linked to a decrease in the scaffold mechanical properties. Mechanically, this was shown to be the result of buckling of the lamellar walls. The pore area increase was suggested to be the result of the formation of clathrate hydrates in the freezing process due to their known presence in frozen IPA–H₂O binary mixtures [25]. While this proposed mechanism is supported by previous literature on IPA–H₂O binary mixtures under steady state conditions, there is no current evidence of clathrate hydrates forming at the high cooling rates observed during the freeze casting process.

In this work we build upon our previous experience on IPA–H₂O freeze casting [14]. We propose the use of IPA–H₂O freeze casting as a simple method to create bioinspired structural composite materials. Additionally, evidence is presented to prove that clathrate hydrates are indeed forming in the freeze casting process and aiding in the creation of enlarged pores. In order to isolate the effect of the IPA–H₂O freezing agent, freeze cast scaffolds were based in zirconia (ZrO₂), which has applications as porous solid oxide fuel cells, thermal barrier layers and for biological implants [26].

1.1. IPA clathrate hydrates

Clathrate hydrates are defined as non-stoichiometric structures where a hydrogen bonded molecule enclosure lattice (H₂O) surrounds a guest molecule (e.g. IPA) with limited or no chemical bonding to the lattice [27]. While most clathrate hydrates are thermodynamically unstable at room temperature and ambient pressure, there are a number of H₂O based solutions that produce clathrates at low temperatures or high pressures. Commonly reported clathrate hydrates include propane–H₂O, which has been heavily studied for its effect on the oil and gas industry [28] and methane–H₂O, which is commonly found at the bottom of the ocean [29]. In addition, binary systems of IPA–H₂O have been reported to form clathrate hydrates at low temperatures and ambient pressures [25,30–33].

In general, clathrate hydrates are capable of forming into a number of different structures depending on the guest molecule size, chemistry and environmental conditions (e.g. pressure and temperature). However, most known clathrate hydrates form either into a structure I (*h*₁) or structure II (*h*₂). These structures are differentiated by their stacking and guest molecule cavity size with *h*₁ stacking on enclosure vertices and *h*₂ stacking on enclosure faces [28]. In the binary IPA–H₂O system, stable clathrate hydrates form at an IPA concentration of 46 vol.% as an *h*₁ structure at 243 K, which converts to *h*₂ at 223 K. The phase diagram displaying this mixture is shown in Fig. 1a. Aladko et al. [25] reported on the *h*₁ and *h*₂ clathrate hydrates of the IPA–H₂O system and determined that, in both cases the hydrophilic hydroxyl group of the guest IPA molecule replaces one of the H₂O molecules in the enclosure lattice. This results in a cubic *h*₁ unit cell with *a*₀ = 1.26 nm and a tetragonal *h*₂ unit cell with *a*₀ = 0.64 nm and *c*₀ = 1.12 nm. Both clathrate unit cells are significantly larger than pure (hexagonal) ice where *a*₀ = ~0.45 nm and *c*₀ = ~0.73 nm. [34]. Diagrams representative of the unit cells found in the IPA–H₂O binary phase diagram are shown in Fig. 1b.

2. Materials and methods

2.1. Sample preparation

Aqueous slurries were prepared with IPA to investigate the effects of monofunctional alcohols as additives to the freeze casting process. Slurries consisting of 10 vol.% ZrO₂ powders

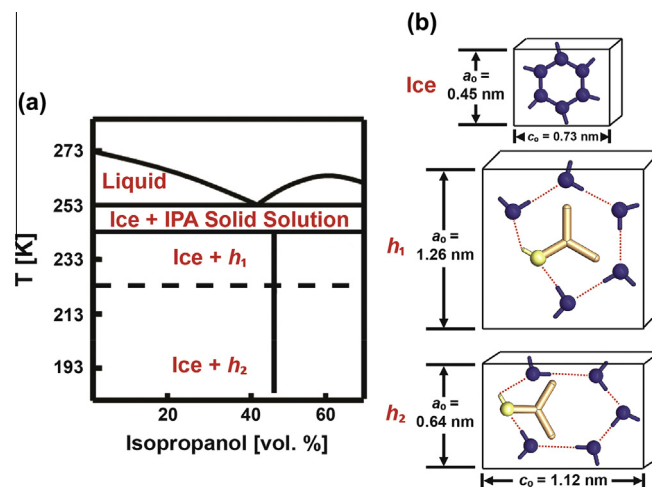


Fig. 1. Phase diagram showing relevant features and unit cells for the IPA–H₂O system at steady state. (a) Stable clathrate hydrates form at 46 vol.% IPA with an *h*₁ forming at 243 K then converting to an *h*₂ at 223 K; (b) Diagrams representative of the known unit cells for features of the IPA–H₂O phase diagram: hexagonal ice (*a*₀ = ~0.45 nm, *c*₀ = ~0.73), *h*₁ clathrate hydrate (cubic, *a*₀ = 1.26 nm) and *h*₂ clathrate hydrate (tetragonal, *a*₀ = 0.64 nm, *c*₀ = 1.12 nm). H₂O molecules are shown in dark blue, IPA molecules are shown in brown (the aliphatic group) and yellow (the hydroxyl group). Phase diagram and clathrate hydrate unit cell data adapted from Aladko et al. [25], hexagonal ice unit cell data adapted from Rottger et al. [34]. (For interpretation of the references to color in this figure legend, the reader is referred to the web version of this article.)

(200–500 nm diameter) (Sigma Aldrich, St. Louis, MO, USA) were mixed with 2 wt.% polyethylene glycol (PEG) with a molecular weight of 10,000 g/mole (Alfa Aesar, Ward Hill, MA, USA) and 1 wt.% of an ammonium polymethacrylate anionic dispersant, Darvan 811 (R.T. Vanderbilt Company, Inc., Norwalk, CT, USA). Eleven slurries were prepared by changing the volume fraction of IPA (J.T. Baker, Center Valley, PA, USA) with the concentrations of 0, 1, 3, 4, 5, 6, 7, 8, 10, 15 and 20 vol.% IPA. All slurries were ball milled in an alumina grinding media for 24 h then degassed under low vacuum for 5–10 min. Samples of approximately 10 mL of the degassed slurry were poured into a freeze cast mold and frozen at a constant rate of 10 K/min using a custom built freeze casting device, as previously described [18]. After freezing, samples were lyophilized in a bench-top freeze dryer (Labconco, Kansas City, MO, USA) at 223 K and 350 Pa for 70 h. Immediately after freeze drying, the green scaffolds were sintered in an open air furnace for 3 h at 1623 K with heating and cooling rates of 2 K/min. This sintering procedure is similar to procedures reported as effective for ZrO₂ scaffolds [18] and through experimentation provided stable but highly porous scaffolds. This process was repeated in order to prove reproducibility of the results.

After sintering, all scaffolds were infiltrated with a two part polymer epoxy, Epoxicure (Buehler, Lake Bluff, IL, USA) by *in situ* polymerization in order to form a ceramic–polymer composite for imaging and mechanical testing. Samples were immersed in a mixture of liquid monomer and catalyst under vacuum (~0.02 Pa) for 20–30 min in order to force the liquid to infiltrate the scaffold pores. The infiltrated scaffolds were then allowed to polymerize for 24 h. At the same time, samples of pure epoxy were created to use as a baseline for mechanical properties.

2.2. Material characterization

All composite scaffolds were observed with scanning electron microscopy (SEM) at 10 kV and a spot size of 3.0 nm using a Philips XL30 field emission environmental scanning electron microscope (FEI Company, Hillsboro, OR, USA). For SEM preparation, all

samples were sputter-coated with iridium using an Emitech K575X sputter coater (Quorum Technologies Ltd., West Sussex, UK). Microstructure measurements of the pore sizes observed in each scaffold were performed using ImageJ software (National Institutes of Health, Bethesda, MD, USA). For each scaffold, $N = 40$ individual pores were measured in order to calculate a mean pore size/shape and standard deviation. Measurements of pore size and shape were performed by adjusting the threshold of the micrographs (using a consistent threshold for all measurements) so as to fit an ellipse to the pores in order to determine the elliptic major axis, a , and minor axis, b . The assumption of elliptical pores has been previously employed for scaffolds with similar architecture [14] and was supported through observations of the pore shape within the current scaffolds. Pore area, A_p , and pore aspect ratio, X_p , were calculated as $A_p = ab\pi/4$ and $X_p = a/b$ respectively. In order to image the characteristic pore structure, samples were taken from the interior of the composite scaffold so as to avoid the high-density regions at the edges, top and bottom of the sample.

Compression testing of the infiltrated scaffold composites was performed using a 3367 Instron materials testing machine (Instron, Norwood, MA, USA) with a 30 kN static load cell at a crosshead velocity of 0.005 mm/s. Scaffolds were cut into cubic samples of roughly $5 \times 5 \times 5 \text{ mm}^3$ and compressed in the longitudinal (ice growth) direction. For each scaffold $N = 5$ samples were tested in order to calculate the mean and standard deviation. In addition samples of pure epoxy were tested. The ultimate compressive strength and effective elastic modulus were determined from the maximum stress and linear slope of the stress–strain curves respectively.

2.3. Differential scanning calorimetry

The phase transformations during freezing of binary mixtures of IPA–H₂O were investigated using a Q20 Differential Scanning Calorimeter (DSC) (TA Instruments, New Castle, DE, USA). DSC has been previously used to investigate phase transformations during the freezing of binary non-hydrogen bonded liquids (e.g. IPA) and H₂O [25,30,31,33,35]. Concentrations of 0, 1, 3, 5, 6, 7, 10 and 15 vol.% IPA were tested with heating and cooling rates of 10 K/min from room temperature to 213 K so as to imitate the freeze casting process. To ensure that this lower temperature limit was satisfactory to simulate the freeze casting process, experiments were conducted by placing thermocouples in a slurry during the freeze casting process, using the procedure outlined above. These experiments determined that at a point ~20 mm from the surface of the slurry (roughly where samples are extracted from the final scaffold), the temperature only reached a minimum of ~210 K by the end of the freeze casting process.

DSC results were quantitatively analyzed by applying a linear integration method to determine the area under the peaks and dividing by the mass of each sample so as to determine the enthalpy of each transition. Results were focused on the two observed endotherms: the h_1 clathrate hydrate endotherm and the hexagonal ice endotherm.

3. Results and discussion

3.1. Structural characterization

ZrO₂ scaffolds fabricated with 0–15 vol.% IPA and infiltrated with epoxy are shown in Fig. 2 showing a significant increase in the pore area up to 5–7 vol.% IPA, then a decrease. Pore area and aspect ratio are shown in Fig. 3a and minor axis and lamellar wall thickness in Fig. 3b as a function of IPA concentration. The pore area undergoes a clear increase from 0 to 5 vol.% IPA (Fig. 2a–c)

as well as a decline from 7 to 15 vol.% IPA (Fig. 2d–f). Of significance, the pore area between 5 and 7 vol.% IPA remains constant while the aspect ratio decreases. From measurements of the pore size and shape, this is due to widening of the pores at 7 vol.% (increase in b seen from 5 to 7 vol.% IPA, as shown in Fig. 3b). Additionally, the lamellar wall thickness increases up to ~8 vol.% IPA before declining (Fig. 3b).

The trend in pore area in IPA–H₂O freeze cast scaffolds with an increase to a maximum value at ~5 vol.% followed by a decline to a base level (the level observed with no additive) matches the previous report for TiO₂ scaffolds with the same solid loading [14]. This consistent result provides evidence that this effect is influenced by the characteristics of the ice formed and is not simply an effect of the solid loading.

This effect was further explored through DSC, as shown in Fig. 4a. Heating curves are displayed overlaid in order to highlight the observed trends with increasing IPA concentration. As is reported in literature [25,30,31,33,35], the phases present are determined through the decomposition observed upon heating of a solid, which correspond to first order phase transformations. The baseline is distilled water (0 vol.% IPA) that displays a large, single endothermic peak corresponding to melting of ice at 273 K (Fig. 4b). With the addition of 1 vol.% IPA, this sharp transition expands and shifts to lower temperatures, thus decreasing the onset of melting below 273 K. Additionally, a secondary endothermic peak beginning at ~243–247 K becomes visible at 3 vol.% IPA and increases in magnitude with greater IPA concentration, though it always occurs at ~243 K. The endotherm is attributed to decomposition of h_1 to a solid solution of ice and IPA, as seen in Fig. 4b [25,33].

The change in enthalpy of each of the two observed endotherms (the h_1 clathrate hydrate and the ice + IPA solid solution) is displayed as a function of IPA concentration in Fig. 5. As expected, as the IPA concentration increases, the enthalpy change of the h_1 endotherm increases and the ice endotherm decreases. This correlates with phase diagram analysis using the lever rule that shows as the amount of IPA increases, the amount of h_1 also increases. However, the h_1 endotherm has a larger rate of change with IPA concentration, up to 5 vol.% IPA, where the maximum in pore area is observed. The rate then decreases above 5 vol.% IPA. The presence of the two different slopes indicates that there is a difference in the nature of the clathrate hydrate formation above and below 5 vol.% IPA. This reduction in the enthalpy of the h_1 clathrate hydrate per unit of IPA (the slope) is correlated to the observed maximum in pore area at 5 vol.% IPA. It is hypothesized that this is due to non-equilibrium behavior of the IPA in solution below 5 vol.% IPA where the IPA molecules are fully dispersed. This gives way to equilibrium behavior (as predicted by the phase diagram) at higher concentrations where IPA molecules in suspension begin to agglomerate.

These results confirm the formation of h_1 , rather than h_2 clathrate hydrates during the current freeze casting process. The proposed process for the increase in pore area due to the observed formation of h_1 clathrate hydrates is diagrammed in Fig. 6.

This drastic increase in pore area provides significant potential for the creation of bioinspired composites by easing infiltration of a second phase. Additionally, the observed decrease in the pore aspect ratio at the maximum pore area between 5 and 7 vol.% may provide insight into the potential for some control of the pore aspect ratio while maintaining high area pores.

3.2. Mechanical characterization

The ultimate compressive strength (UCS) and compressive modulus of infiltrated ZrO₂–epoxy two phase composites are shown in Fig. 7 as a function of IPA additive. In both cases the

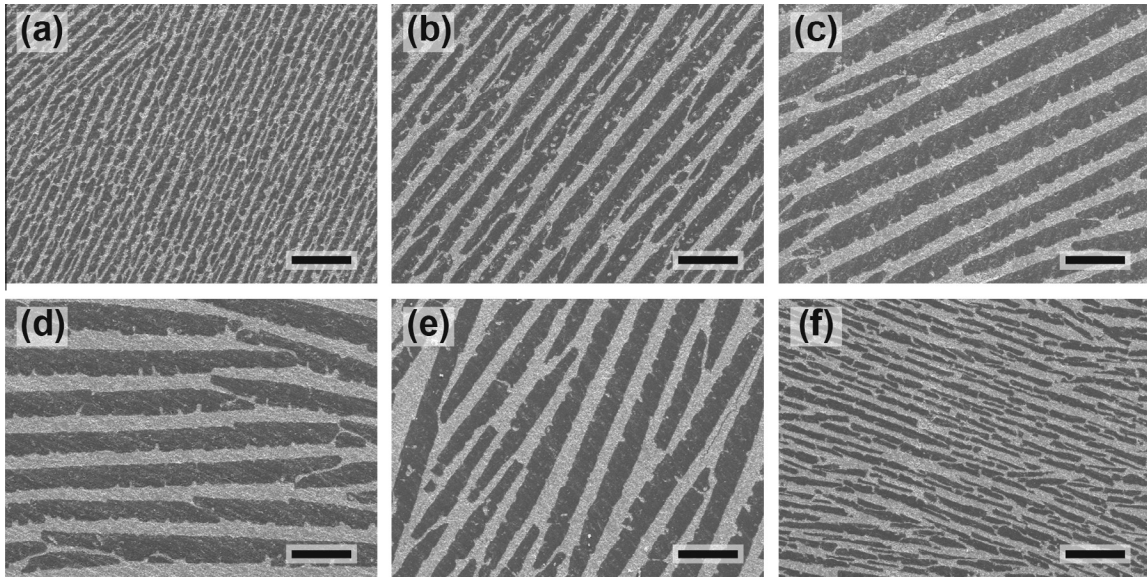


Fig. 2. Scanning electron microscopy images of epoxy infiltrated ZrO_2 scaffolds. IPA concentration: (a) 0 vol.%; (b) 1 vol.%; (c) 5 vol.%; (d) 7 vol.%; (e) 10 vol.%; (f) 15 vol.%. Ceramic is shown in light gray, polymer in dark gray. Scale bars: 100 μm .

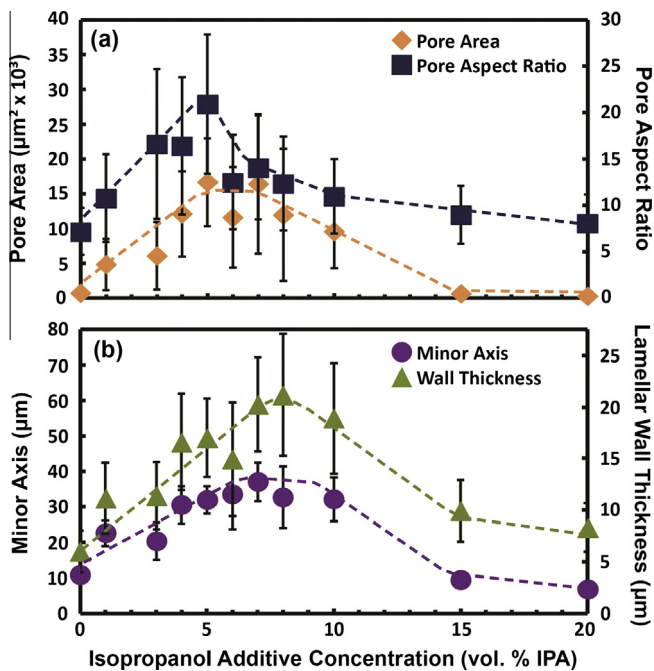


Fig. 3. Pore area, aspect ratio, minor axis and lamellar wall thickness as a function of IPA additive concentration. (a) Pore area shows a maximum at 5–7 vol.% IPA while pore aspect ratio shows a maximum at 5 vol.% IPA and a sharp decline at 6–7 vol.% IPA; (b) both minor axis and lamellar wall thickness reach a maximum at ~ 7 –10 vol.% IPA. Data points are the mean of $N = 40$ measurements with error bars representing \pm one standard deviation.

mechanical properties experience an increase up to ~ 5 vol.% IPA then remain relatively constant up to 20 vol.%. The addition of IPA increases the mechanical properties above those of the epoxy, a phenomena that is commonly observed in complex biological two-phase composite materials [4]. Previous work demonstrated that the failure mode of scaffolds in the longitudinal (ice growth) direction is buckling of the lamellar walls [14]. For comparison, these previous results, performed on non-infiltrated TiO_2 freeze cast scaffolds of the same solid loading (10 vol.%) and IPA as an

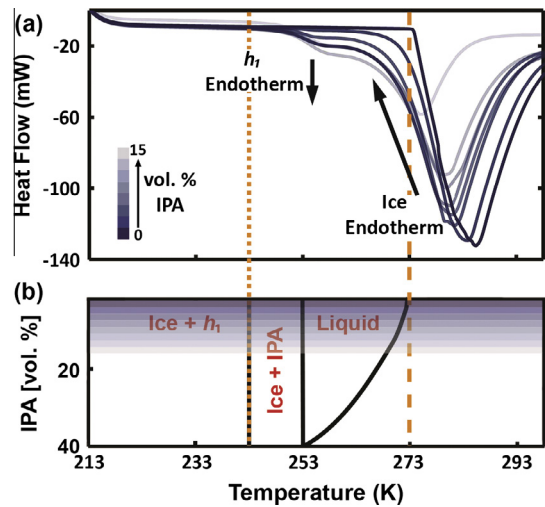


Fig. 4. Differential scanning calorimetry results taken during heating for varying concentrations of IPA in H_2O . (a) Data is overlaid to show the general trends with increasing IPA concentration. Note the decrease in magnitude and shift to lower temperatures of the ice (ice + IPA solid solution) endotherm as well as the emergence of an h_1 clathrate hydrate endotherm beginning at ~ 243 –247 K as IPA concentration increases; (b) for reference, the IPA– H_2O equilibrium phase diagram is shown to highlight the transitions occurring at 273 K (melting of ice) and 243 K (decomposition of h_1 clathrate hydrate into ice + IPA solid solution).

additive are shown in Fig. 7. The contrasting observed increase in the mechanical properties of the infiltrated scaffolds seen in Fig. 7 suggests that, in addition to adding mechanical toughness, the polymer phase supports the lamellar walls and inhibits buckling. The leveling out of the mechanical properties above 5 vol.% IPA can be attributed to several competing factors: although the porosity decreases, which should increase the strength and modulus, the lamellar wall thickness also decreases, which should decrease the strength and modulus.

Although the mechanical properties of the ZrO_2 -epoxy composites are not exceptionally high (Fig. 7) the relative increase in strength and stiffness above those of the initial constituents suggests that infiltration with different materials (e.g. metal melts)

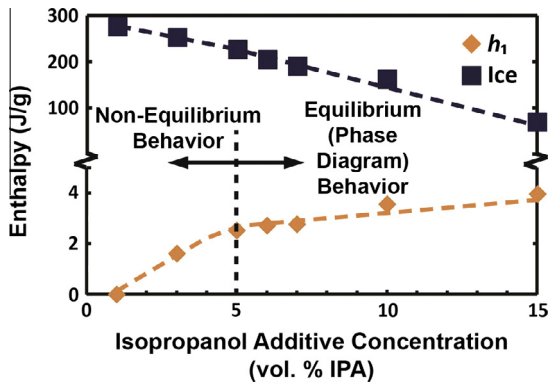


Fig. 5. Enthalpy of the transitions observed from the differential scanning calorimetry results as a function of IPA concentration. As vol.% IPA increases, the enthalpy of the h_1 clathrate hydrate endotherm increases with a high initial slope up to 5 vol.% then a lower slope. Inversely, the enthalpy of the ice + IPA solid solution endotherm (ice) decreases with increasing IPA concentration. It is proposed that the change in slope occurs due to non-equilibrium behavior of the IPA in solution at concentrations below 5 vol.% that gives way to equilibrium behavior (as expected from the phase diagram) at high concentrations.

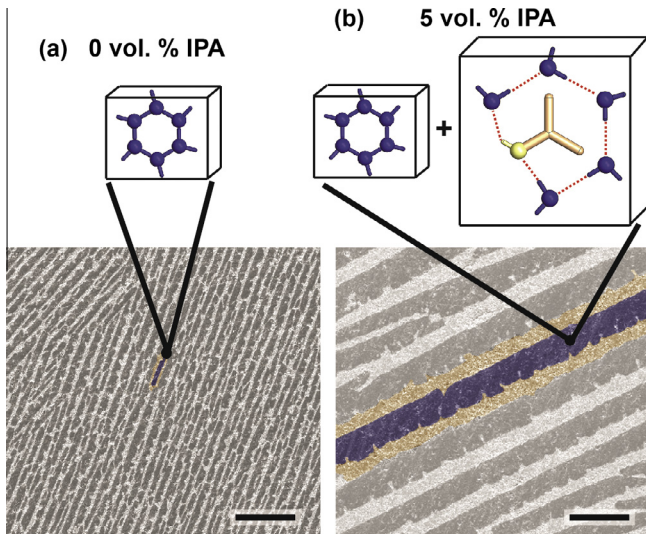


Fig. 6. Diagram of the proposed mechanism for the observed increase in pore size due to the formation of h_1 IPA–H₂O clathrate hydrates during the freezing process. (a) At 0 vol.% IPA, only hexagonal ice forms, resulting in smaller pore sizes; (b) at 5 vol.% IPA, the formation of both hexagonal ice and the enlarged h_1 clathrate hydrate result in significantly enlarged pores. Scale bars: 100 μ m.

could result in more high performance composites for a variety of structural applications. As a result, the infiltration of IPA–H₂O freeze cast scaffolds with a variety of constituents warrants further investigation. More importantly, these results suggest that the use of IPA in the freeze casting process is a simple and beneficial method for the creation of bioinspired composites with enlarged porous microstructures.

4. Conclusions

The current experimental study of epoxy-infiltrated, freeze cast ZrO₂ bioinspired composites using isopropanol (IPA)–H₂O as a freezing agent enables the following conclusions.

- The IPA–H₂O system showed an increase in pore area up to a maximum at ~5–7 vol.% IPA then a decrease. This result was previously shown for similar freeze casting experiments with

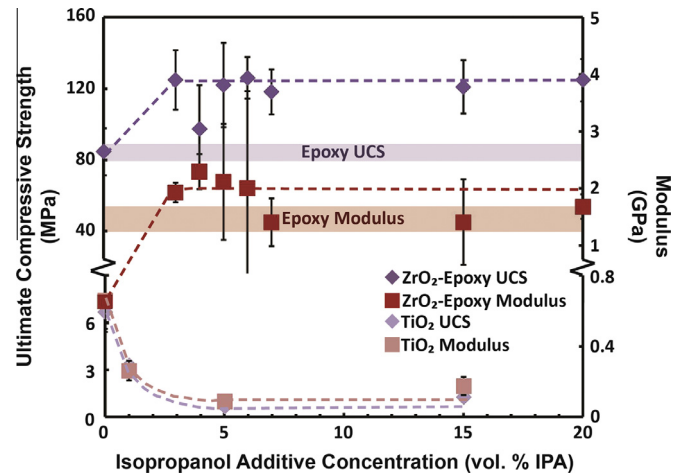


Fig. 7. Ultimate compressive strength (UCS) and compressive modulus of freeze cast ZrO₂-epoxy composites as a function of IPA additive concentration. In both cases the mechanical properties experience a rise with the IPA additive then remain relatively constant up to 20 vol.% IPA. Compressive modulus and UCS for the pure epoxy are shown (band = mean \pm standard deviation of $N = 5$ measurements) for reference. Data is compared to previous reports on non-infiltrated freeze cast TiO₂ scaffolds with the same solid loading and IPA as an additive [14] that show a decrease in UCS and modulus with increasing IPA additive concentration. Data points are the mean of $N = 5$ measurements with error bars representing \pm one standard deviation.

TiO₂ as the solid loading and therefore suggests that the effect is strongly influenced by the freezing agent and is not solely an effect of the solid loading. Additionally, little change was observed in the pore area of the scaffolds between 5 and 7 vol.% IPA, however the aspect ratio showed a large decrease due to widening of the pores.

- Differential scanning calorimetry experiments that mimic the freeze casting process showed that h_1 clathrate hydrates are present during freezing of IPA–H₂O binary mixtures. These h_1 clathrate hydrates are shown to be the cause of the enlarged pores observed in the resultant freeze cast scaffolds.
- Analysis of the change in enthalpy of the h_1 clathrate hydrate to an ice + IPA solid solution show that the maximum in pore area is physically caused by the reduction in slope (enthalpy of the h_1 clathrate hydrate per unit of IPA). It is currently hypothesized that this is due to un-saturated behavior of the IPA in solution below 5 vol.% IPA, which gives way to saturated behavior (as predicted by the phase diagram) at higher concentrations.
- Mechanical properties (ultimate compressive strength and compressive modulus) of two-phase, bioinspired ZrO₂-epoxy composites showed an increase with the addition of the IPA additive up to 5 vol.%, which then remained relatively constant up to 20 vol.%. Similar to many biological two-phase composites, these mechanical properties were higher than what would be expected from a simple mixture of the two constituents. This suggests that the infiltration of freeze cast scaffolds will inhibit the reported failure mode of lamellar wall buckling and increase the mechanical properties.

Acknowledgments

This work is supported by a UC San Diego Academic Senate Bridge Grant (2013–2014) and a Multi-University Research Initiative through the Air Force Office of Scientific Research of the United States (AFOSR-FA9550-15-1-0009). The authors wish to acknowledge Yi-Hsuan Hsiao and Michael B. Frank for their help in the freeze casting process.

References

- [1] Ritchie RO, Kinney JH, Kruzic JJ, Nalla RK. A fracture mechanics and mechanistic approach to the failure of cortical bone. *Fatigue Fract Eng Mater Struct* 2005;28:345–71.
- [2] Lopez MI, Chen P-Y, McKittrick J, Meyers MA. Growth of nacre in abalone: seasonal and feeding effects. *Mater Sci Eng, C* 2011;31:238–45.
- [3] Meyers MA, Lin YS, Olevsky EA, Chen P-Y. Battle in the amazon: arapaima versus piranha. *Adv Biomater* 2012;14:B279–88.
- [4] Munch E, Launey ME, Alsem DH, Saiz E, Tomsia AP, Ritchie RO. Tough, bio-inspired hybrid materials. *Science* 2008;322:1516–20.
- [5] Deville S, Saiz E, Nalla RK, Tomsia AP. Freezing as a path to build complex composites. *Science* 2006;311:515–8.
- [6] Porter MM, McKittrick J, Meyers MA. Biomimetic materials by freeze casting. *JOM* 2013;65:720–7.
- [7] Clarke DR. Interpenetrating phase composites. *J Am Ceram Soc* 1992;75:739–59.
- [8] Deville S, Saiz E, Tomsia AP. Freeze casting of hydroxyapatite scaffolds for bone tissue engineering. *Biomaterials* 2006;27:5480–9.
- [9] Bouville F, Maire E, Meille S, Van de Moortele B, Stevenson AJ, Deville S. Strong, tough and stiff bioinspired ceramics from brittle constituents. *Nat Mater* 2014;13:508–14.
- [10] Deville S. Ice-templating, freeze casting: beyond materials processing. *J Mater Res* 2013;28:2202–19.
- [11] Deville S. Freeze-casting of porous ceramics: a review of current achievements and issues. *Adv Eng Mater* 2008;10:155–69.
- [12] Deville S, Maire E, Lasalle A, Bogner A, Gauthier C, Leloup J, et al. Influence of particle size on ice nucleation and growth during the ice-templating process. *J Am Ceram Soc* 2010;93:2507–10.
- [13] Hunger PM, Donius AE, Wegst UGK. Structure–property–processing correlations in freeze-cast composite scaffolds. *Acta Biomater* 2013;9:6338–48.
- [14] Porter MM, Imperio R, Wen M, Meyers MA, McKittrick J. Bioinspired scaffolds with varying pore architectures and mechanical properties. *Adv Funct Mater* 2013;24:1978–87.
- [15] Munch E, Saiz E, Tomsia AP, Deville S. Architectural control of freeze-cast ceramics through additives and templating. *J Am Ceram Soc* 2009;92:1534–9.
- [16] Korber C, Rau G. Interaction of particles and a moving ice-liquid interface. *J Cryst Growth* 1985;72:649–62.
- [17] Zhang Y, Hu L, Han J. Preparation of a dense/porous bilayered ceramic by applying an electric field during freeze casting. *J Am Ceram Soc* 2009;92:1874–6.
- [18] Porter MM, Yeh M, Strawson J, Goehring T, Lujan S, Siripasopsotorn P, et al. Magnetic freeze casting inspired by nature. *Mater Sci Eng, A* 2012;556:741–50.
- [19] Binner J, Chang H, Higginson R. Processing of ceramic–metal interpenetrating composites. *J Eur Ceram Soc* 2009;29:837–42.
- [20] Chen HM, Yin YF, Dong HB, Tong Y, Luo M, Li X. Porous alumina infiltrated with melt and its dynamic analysis during pressureless infiltration. *Ceram Int* 2014;40:6293–9.
- [21] Rao BS, Jayaram V. New technique for pressureless infiltration of Al alloys into Al₂O₃ preforms. *J Mater Res* 2001;16:2906–13.
- [22] Porter MM, Lee S, Tanadchangsang N, Jaremko MJ, Yu J, Meyers MA, et al. Porous hydroxyapatite-polyhydroxybutyrate composites fabricated by a novel method via centrifugation. *Mech Biol Syst Mater* 2013;5:63–71.
- [23] Launey ME, Munch E, Alsem DH, Barth HB, Saiz E, Tomsia AP, et al. Designing highly toughened hybrid composites through nature-inspired hierarchical complexity. *Acta Mater* 2009;57:2919–32.
- [24] Russias J, Saiz E, Nalla RK, Gryn K, Ritchie RO, Tomsia AP. Fabrication and mechanical properties of PLA/HA composites: a study of in vitro degradation. *Mater Sci Eng, C* 2006;26:1289–95.
- [25] Aladko LS, Mankov AY, Ogienko AG, Ancharov AI. New data on phase diagram and clathrate formation in the system water–isopropyl alcohol. *J Incl Phenom Macrocycl Chem* 2009;63:151–7.
- [26] Hench LL. Bioceramics – from concept to clinic. *J Am Ceram Soc* 1991;74:1487–510.
- [27] van der Waals JH, Platteeuw JC. Clathrate solutions. *Adv Chem Phys* 1959;2:1–57.
- [28] Englezos P. Clathrate hydrates. *Ind Eng Chem Res* 1993;32:1251–74.
- [29] Klapp SA, Bohrmann G, Kuhs WF, Murshed MM, Pape T, Klein H, et al. Microstructures of structure I and II gas hydrates from the Gulf of Mexico. *Mar Pet Geol* 2010;27:116–25.
- [30] Murthy SSN. Detailed study of ice clathrate relaxation: evidence for the existence of clathrate structures in some water–alcohol mixtures. *J Phys Chem A* 1999;103:7927–37.
- [31] Ott JB, Goates JR, Waite BA. (Solid + liquid) phase-equilibria and solid-hydrate formation in water + methyl, + ethyl, + isopropyl, and + tertiary butyl alcohols. *J Chem Thermodynam* 1979;11:739–46.
- [32] Potts AD, Davidson DW. Ethanol hydrate. *J Phys Chem* 1965;69:996–1000.
- [33] Takaizumi K. Liquid–solid phase diagrams of PrOH–water and BuOH–water systems from differential scanning calorimetry. *J Solution Chem* 2000;29:377–88.
- [34] Rottger K, Endriss A, Ihringer J, Doyle S, Kuhs WF. Lattice-constants and thermal-expansion of H₂O and D₂O ice Ih between 10 and 265 K. *Acta Crystall B* 1994;50:644–8.
- [35] Manakov AY, Aladko LS, Ogienko AG, Ancharov AI. Hydrate formation in the system *n*-propanol–water. *J Therm Anal Calorim* 2013;111:885–90.